Optics, morphology, and growth kinetics of GaAs/$Al_xGa_{1-x}As$ quantum wells grown on vicinal substrates by metalorganic vapor phase epitaxy

N. Moret, D. Y. Oberli, E. Pelucchi,* N. Gogneau,† A. Rudra, and E. Kapon
Ecole Polytechnique Fédérale de Lausanne (EPFL), Laboratory of Physics of Nanostructures, CH-1015 Lausanne, Switzerland
(Received 21 July 2011; revised manuscript received 16 September 2011; published 17 October 2011)

The effect of the miscut angle of vicinal substrate on the optical and morphological properties of GaAs/$Al_xGa_{1-x}As$ quantum wells grown by metalorganic vapor phase epitaxy is studied by means of photoluminescence (PL) and atomic force microscopy. Within small changes of the miscut angle, we observe strong variations of the PL linewidth, energy, and lineshape, as well as transitions between the morphology of the sample's surface and interface. The relation between these features is discussed, and the particular case of structures exhibiting high optical quality is studied in more detail. Moreover, the role of growth dynamics is highlighted by observing the evolution of the hetero-interfaces during growth interruption.

DOI: 10.1103/PhysRevB.84.155311 PACS number(s): 78.55.Cr

I. INTRODUCTION

The homogeneity of quantum well (QW) heterostructures has benefited from constant progress since the first structures were grown in the 1970's. Amongst the indicators of QW quality, the broadening of the photoluminescence (PL) line has always been the most widely used because it is the most straightforward criterion that bears high sensitivity to the structural features. The relationship between the interfaces of QWs and the resulting PL has long been at the center of rich debates.[1–6] There now exists a largely accepted picture of the disorder of the interfaces, which is effectively modeled in terms of a two-length-scale roughness at the interfaces.[7–9]

Although occurring on a scale close to the Angström, the short-range fluctuations of the hetero-interface composition or geometry are usually referred to as microroughness. Arising from the random distribution of atoms in an alloy or the interdiffusion of atoms between layers of different compositions, it occurs on a range smaller than the exciton Bohr radius a_B, which governs the optical properties. Such fluctuations are therefore smoothed out in the optical spectra.[10] Besides, some mesoscopic structure may appear at a larger length scale. Such patterns are found in various epitaxially grown materials, and the theoretical modeling of their formation is rather well established.[11–18] The variations of the QW width resulting from the peculiar morphology of these mesostructures are no more averaged over the exciton extension. They thus may lead to localization of the exciton, manifested by the appearance of distinct lines in the PL spectra that are commensurate with the varying effective QW width.[19] Narrow PL linewidths therefore correspond to homogenous QW interfaces over a length scale larger than a_B.

Even if the fabrication of such homogeneous QW systems remains a challenge, some methods have been successfully employed to control to a certain extent the morphology of epitaxial layers. A growth interruption (GI) at an interface allows the layer to reach an equilibrium morphology. Extensively used in molecular beam epitaxy (MBE), this technique has allowed the formation of atomically flat interfaces over micron-long distances[20] enabling the preparation of high optical quality QWs.[21–23]

The use of vicinal substrates has also been extensively investigated as a way to modify the growth mode.[24–27] For metalorganic vapor phase epitaxy (MOVPE), with appropriate growth conditions, a significant reduction of the PL linewidth was found for QWs grown on substrates with a small miscut angle.[28] This was tentatively explained by the interplay between the abruptness and morphology of the miscut-dependent QW interfaces, based on atomic force microscopy (AFM) characterization of the sample surfaces.[29]

However, direct correlations between QW interface morphology and optical properties are still subject to discussions. When comparing the effect of GI in various MBE samples, Leosson *et al*. noticed the contradiction between the smooth as-grown sample surfaces and the apparent microroughness deduced from PL.[23] Indeed, the morphology of the QW interfaces has been shown to differ significantly from that observed on the cooled-down surface.[30] The technique reported in Ref. 30, employed to uncover the real QW interfaces, allowed a direct comparison between the morphology and the physical properties of MBE-grown QWs. The same method was used to study the growth kinetics in MOVPE and recently allowed to correlate the growth features to the optical properties.[31]

In this paper, we first report the large variations of the optical properties of QWs grown by MOVPE on vicinal substrates, which miscut angle spans the range [0°, 8°]. In particular, we demonstrate that very narrow PL linewidth (0.5 meV for a 15-nm-thick QW) can be obtained on substrates with a small miscut angle (∼0.2°); this allows us to resolve exciton complexes in the PL spectra. We then use a modified structure to investigate the real QW interface morphology and show that the growth mode on 0.2°-off substrates can be characterized by step flow, in contrast to what would be deduced from the observation of the cooled-down sample surface. We observe several different morphologies within a small miscut angle range and are able to correlate them directly to the corresponding PL spectra. Finally, we discuss the transitions between the diverse growth modes in view of the existing growth models.

II. EXPERIMENTAL

A. Samples

The vicinal GaAs/$Al_xGa_{1-x}As$ QW samples were grown in a low-pressure MOVPE reactor at a substrate temperature of 690 °C with large (from 120 to 280 depending on the layers) V/III ratio. All samples discussed in this paper were grown on (001)-GaAs substrates misoriented towards the [111]A direction. Such miscuts result in the formation of Ga-rich A-steps on vicinal surfaces. As A-steps are usually smoother than As-rich B-steps, growth is expected to result in better defined interfaces. More details on the growth conditions and their role can be found in Ref. 28.

We used three types of structures in our experiments. The triple QW (TQW) structure consists of three GaAs QWs of 15-, 5-, and 2-nm thickness, separated by 300-nm-thick $Al_{0.3}Ga_{0.7}As$ barriers and covered by a 30-nm GaAs capping layer. This structure is optimized for optical measurements and allows imaging of the surface morphology. To investigate the interior interfaces of the QWs, we designed a double QW (DQW) structure (a schematic is summarized in Table I for clarity). Here, the first QW (QW1, 15 nm) is covered by a 300-nm AlAs layer, whereas its lower barrier consists of a 300-nm-thick $Al_{0.3}Ga_{0.7}As$ layer. The second QW (QW2, 5 nm) is grown below QW1 and has two 300-nm-thick $Al_{0.3}Ga_{0.7}As$ barriers, similar to the case of the TQW structure. However, the upper interface of QW2 is covered by five monolayers (MLs) of AlAs to ensure that the surface features occurring during the growth of QW1 are preserved.[30] Although the DQW sample is also covered by a 30-nm GaAs cap, its morphology is affected by the thick AlAs layer grown below and cannot be used to compare (morphologically) to samples without the AlAs layers and/or the QW layer as such. The last type of structure (NQW, for no-QW) consists of 300-nm $Al_{0.3}Ga_{0.7}As$ covered by 300-nm AlAs and 30-nm GaAs; it is used for the characterization of the $Al_{0.3}Ga_{0.7}As$ surface morphology.

B. Optical characterization

All optical measurements were done at 10 K with the samples mounted on the cold finger of a helium-flow cryostat. For spatially resolved measurements (micro-PL, μPL), the laser spot was focused through a microscope objective, which also served for collecting the luminescence. The exciting spot diameter was about 1 μm. For standard PL and PL excitation (PLE) spectroscopy, the spot diameter was of the order of 30 μm. We used an argon-ion laser emitting at 514-nm wavelength for PL and μPL excitation and a tunable titanium-sapphire laser for PLE measurements.

TABLE I. Schematic of the double QW system investigated in the text.

Layer	Thickness	Composition
Cap	30 nm	GaAs
Sacrificial barrier	300 nm	AlAs
QW1	15 nm	GaAs
Barrier II	300 nm	$Al_{0.3}Ga_{0.7}As$
Etch selective barrier	5 monolayers	AlAs
QW2	5 nm	GaAs
Barrier I	500 nm	$Al_{0.3}Ga_{0.7}As$
Buffer	500 nm	GaAs
Substrate	~350 μm	GaAs

C. Morphology characterization

The morphology of the QW structures was characterized using AFM in noncontact mode. In order to probe the interior interfaces of the QWs, we used the wet etching technique proposed by Bernatz *et al.*,[32] for which the DQW and NQW structures are designed. The GaAs cap is first removed with NH_3:H_2O_2 (1:150). The upper AlAs barrier is subsequently etched in diluted HF (10% for DQW, 1.5% for NQW), exposing the GaAs interface of QW1 in the DQW structure ($Al_{0.3}Ga_{0.7}As$ interface in NQW). The selectivity of HF is virtually perfect on GaAs. The use of a more dilute HF solution also allows good enough selectivity to evidence the main morphological features on $Al_{0.3}Ga_{0.7}As$. In that latter case, the AFM measurement is performed within a few hours after the etching step in order to minimize the effect of $Al_{0.3}Ga_{0.7}As$ oxidation.

III. OPTICAL PROPERTIES

A. Dependence on substrate miscut

The PL spectra of a series of TQW samples, grown on vicinal substrates, with miscut angle varying between 0° and 8° and measured at an excitation density of ~2 W/cm,[2] are displayed in Fig. 1(a) (logarithmic scale). Three emission lines, emanating from the 15-, 5-, and 2-nm-thick QWs and flanked by features from the bulk GaAs (buffer and substrate) and $Al_xGa_{1-x}As$ (barriers), can be identified. Significant dependence of the spectra on the substrate miscut is observed. If most QWs emit around the expected energy (1.53, 1.61, and 1.74 eV for the 15-, 5-, and 2-nm QW, respectively), with minor fluctuations, for miscuts between 0.6° and 1.2°,

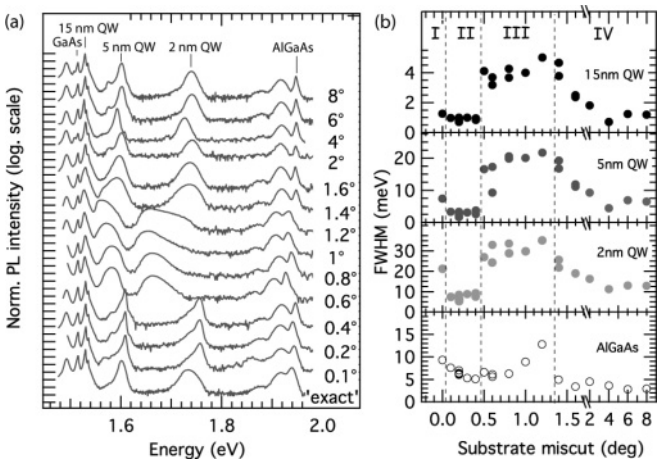

FIG. 1. (a) PL spectra of TQW samples grown on substrates with different miscuts. The intensity scale is logarithmic. (b) FWHM of the three QWs and of the $Al_xGa_{1-x}As$ bound exciton line as a function of the substrate miscut. The PL is excited at 10 K with a 10-μW Ar^+ laser beam.

the QW emission is red shifted, and the line shape changes significantly. Conversely, there is a narrow range of angles, around 0.2°, for which the QW line is slightly blueshifted and is much narrower compared to the other miscuts. We also note some structure on the low-energy side of the PL line shape, especially visible for the 5-nm-thick QWs. This corresponds to impurity-related transitions and does not influence significantly the measurement of the intrinsic linewidth.

The full width at half maximum (FWHM) of the QW PL is displayed as a function of the miscut angle in Fig. 1(b). All three kinds of QWs show the same behavior: for nominally exact (001) samples (angle range I), the linewidth is moderate. It decreases with increasing miscut angle to reach a minimum around 0.2° (range II), for which the lowest values are 0.6, 1.6, and 5.2 meV for the 15-, 5-, and 2-nm QWs, respectively. For intermediate angles (∼0.4°–1.4°, range III), the lines broaden importantly to reach FWHM values more than twice those obtained on exact substrates. Above about 1.4° (range IV), the FWHM decreases again and then remains more or less constant for larger miscut angles, setting at values between those of exact and 0.2°-off samples.

The features of the bulk GaAs and $Al_xGa_{1-x}As$ materials are also affected by the substrate miscut. Only weak differences are seen between the GaAs emission features of the different samples, but the $Al_xGa_{1-x}As$ PL line shape shows significant variations, [lowest panel of Fig. 1(b)]. The $Al_xGa_{1-x}As$ emission consists of spectral features due to the recombination of bound excitons, donor-acceptor pairs, and phonon replica. The bound exciton emission is the highest energy line. Its FWHM also follows a nonmonotonous evolution on the substrate miscut: from about 9 meV on exact substrates, it reduces down to 5 meV before increasing again to more than 12 meV for the 1.2°-off sample and finally decreasing abruptly to reach its smallest value (3 meV) for larger miscuts. Although this behavior is similar to that of the QWs, we note that: (i) the local minimum for small miscut is extended over a larger angle range than for the QWs; (ii) large FWHM values are obtained only within a narrow angle range as compared to the QWs; and (iii) the narrowest linewidths are obtained for large miscut angles.

The peak energy of the $Al_xGa_{1-x}As$ emission is also significantly modified by the substrate miscut, corresponding to fluctuations close to 1% in the Al-content. The FWHM of the lines emitting at the highest energy (for samples of angle range IV) are the narrowest ones. This can be interpreted as a result of the competition between Al atoms and impurities in incorporation into the crystal. However, the above observations indicate that the variations in the PL spectral features of the QWs are not directly triggered by variations of the bulk materials properties.

Figure 2(a) shows PLE spectra, detected at the QW emission peaks, for the 5-nm QWs of typical samples from each angle domains. The first heavy (hh) and light hole (lh) excitonic transitions are well resolved, and their broadening mimics that of the PL lines. The ratio between the intensity of the hh and lh transitions exhibit small differences between the samples. The ratio is larger for the 0.2°-off sample; conversely, the e_1-h_1 transition disappears for the 0.6° sample (this is specific of the 5-nm QW, and unfortunately, we do not have

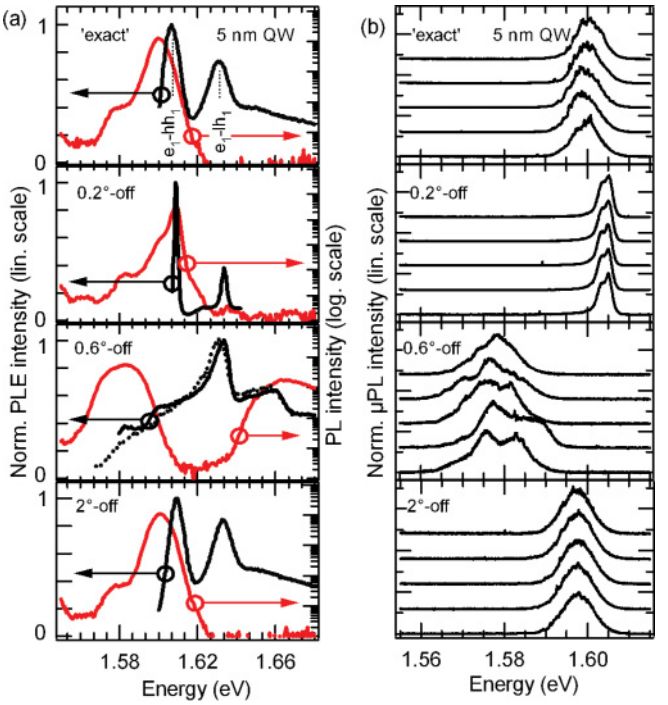

FIG. 2. (Color online) (a) 10 K PL (right log. scale) and PLE (left linear scale) spectra of the QW emissions of four samples from different miscut angle domains. Please note that the second redshifted PL peak in the 0.6°-off sample is originating from the 2-nm QW, see Fig. 1. (b) Representative μPL spectra of the same samples measured at random positions (10 μW Ar^+ laser beam, 10 K).

a clear explanation for this last observation). For the 0.6° sample, two PLE spectra are shown, corresponding to different detection energies: one at the peak (thick line) and the other at energy lower by 15 meV, in the low-energy tail of the PL spectrum (dotted line). No other transition is detected in the latter case. Remarkably, all PLE resonances appear approximately at the same energy. The shift in the PL energy between the samples thus corresponds to a Stokes shift. This points toward various degrees of inhomogeneity in the different samples.

This picture is confirmed by the μPL spectra shown in Fig. 2(b), acquired at random positions of the same samples as in Fig. 2(a). Spectra of the exact and 2°-off samples both consist of a rather broad emission, from which sharp lines emerge. These lines are attributed to localized excitons; they are distributed slightly more homogeneously on the 2°-off sample. On the 0.2°-off sample, the emission is very uniform at all positions. For these excitation conditions (10 K, 10 μW), it displays a low-energy line, the origin of which is discussed in the next paragraph. Finally, μPL allows us to decompose the emission of the 0.6°-off sample, which exhibits a broad and redshifted PL spectrum, into several peaks widely distributed in space and energy.

B. Observation of charged excitons

The narrow PL linewidth of QWs grown on substrates of domain II allows us to resolve a clearly distinct peak, whose intensity relative to the dominant line depends strongly on the excitation conditions. Figure 3(a) shows the μPL spectra of

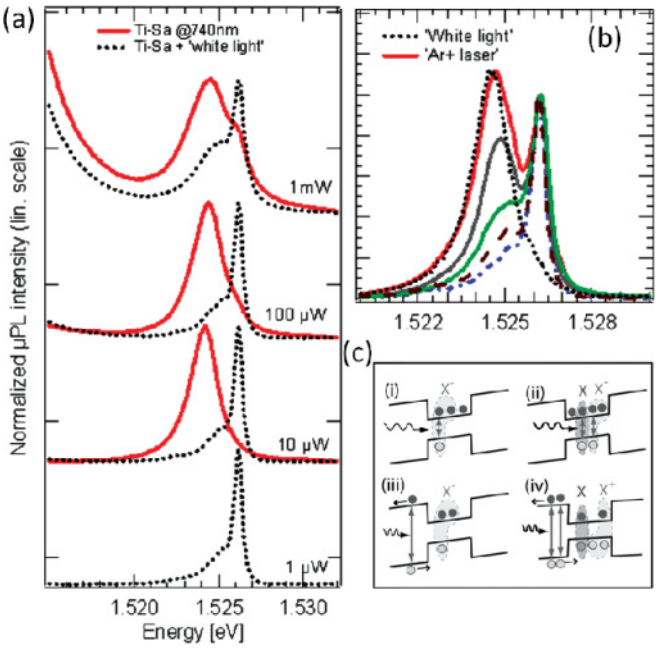

FIG. 3. (Color online) (a) 10 K μPL spectra of a 15-nm QW (0.2°-off) excited below the barrier (740 nm) with increasing power. (b) The same QW excited above barrier at different densities. Increasing line thickness corresponds to increasing intensity. In (a) and (b), dotted lines stand for excitation above barrier of a large area with a white light. (c) Illustration of the charged excitons formation mechanism discussed in the text with two initial excess electrons.

a 15-nm QW grown on a 0.2°-off substrate acquired under different excitation conditions. In panel (a), the thick lines correspond to excitation below the barriers. The dotted-line spectra were obtained by additionally shining light with a wide-spectrum lamp (white light), thus generating carriers in the barriers. The difference is striking: for below-barrier excitation, the μPL is strongly (>1 meV) redshifted and rather broad (1.8 meV FWHM). With increasing power, the line slightly blueshifts, and a shoulder appears at higher energy. This shoulder corresponds to the narrow exciton line, as evidence by Fig. 3(b), in which spectra obtained with white light excitation of increasing intensity are superposed to spectra obtained with Ar^+ laser excitation. For weak white light excitation, the spectrum is comparable to that obtained with Ti-Sa excitation. With additional excitation intensity, the situation is similar to that described in standard PL, in which a large low-energy shoulder increases with excitation power.

Spectral lines appearing on the low-energy side of excitons have been reported in several systems and were attributed to diverse origins. They could correspond to emission from QW areas of different thickness, excitons localized by potential fluctuations,[33–35] excitons bound to impurities,[36] or exciton complexes.[37–39] In our samples, the energy separation (∼1.2 and 2 meV for the 15- and 5-nm QWs, respectively) rules out thickness differences. Localized excitons can be rejected for the same argument. The particular behavior that we observe when varying the excitation conditions (first the saturation of the low-energy component and then the increase of another line) suggests the formation of two types of excitonic complexes.

If electron-hole pairs bind to excess charges in the QW, they form a charged exciton. As the number of excess charges is fixed by the residual doping, the charged exciton line saturates at increasing excitation power. A further increase in intensity may lead to the formation of biexcitons. A biexciton is yet expected to have a larger binding energy than a charged exciton.[40] This fact does not fit our observations. One may therefore consider the saturation of one type of charged exciton (e.g. negatively charged), before the other type (e.g. positively charged) becomes dominant. The binding energy of negatively charged excitons is known to be larger than that of positively charged excitons in QWs and disorder-induced QDs,[39,40] although the values are very close to each other.[41]

In order for this interpretation to fit our observations, it requires the assumption of an initial excess density of electrons in the QW and an increasing number of holes with increasing excitation density. Two mechanisms can be imagined to provide excess charges to the QW. First, the charges can be due to the residual background doping, independently of the excitation conditions. Second, one type of charge can be preferentially captured due to a built-in electric field.

The first mechanism does play a role in our structures, as we observe the low-energy line when we excite below the barriers. The second mechanism is also probably active, as proved by the strong effect of the above-barriers excitation power. The small shifts visible with increasing excitation power also support this affirmation.

This mechanism is illustrated in Fig. 3(c): weak excitation leads to the formation of negatively charged excitons due to the presence of excess electrons (i) and (iii). Additional holes created by increased excitation bind to form neutral excitons, coexisting either with negatively (ii) or positively (iv) charged excitons depending on the band bending and excitation wavelength.

IV. MORPHOLOGY

A. Surface morphology

The surface features of a heterostructure sample are often used as an indicator of its quality. Figure 4(a) shows AFM images and scan profiles of the annealed GaAs surface of TQW samples that are representative of each domain of substrate miscut angle. We observe a broad range of morphology types. The surface of the exact (001) sample shows a step-flow (SF) morphology with ML high terraces, for which width is determined by the local miscut angle. We observed that this angle changes considerably within a single wafer and sometimes exceeds the nominal specification of ±0.02°-off (100). There are no clearly defined terraces on the 0.2°-off surfaces. Instead, the steps merge locally, creating 1–2-ML-high fluctuations. We refer to this morphology as coalescent step bunching (CSB). The sample representing the third miscut angle domain (0.6°-off) shows a different type of step bunching: the steps merge to create multisteps at a more or less regular interval. We term this morphology periodic step bunching (PSB). The height variations are in this case in the nanometer range, and steps are rather straight, although they still mix together locally. Finally, samples with larger miscut angles (domain IV) also exhibit coalescent step bunching,

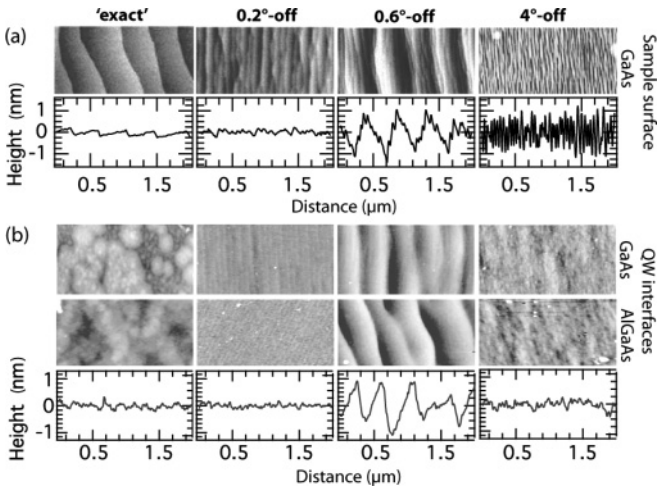

FIG. 4. Here, $2 \times 1\ \mu m^2$ flattened AFM images and representative surface profiles of (a) the GaAs surface of TQW samples and (b) the GaAs and $Al_xGa_{1-x}As$ interfaces of DQW and NQW structures grown on substrates with different miscuts. Respective height scales are 2, 2, 5, and 4 nm in (a) and 2.5, 3, 6, and 3 nm in (b).

although with a larger amplitude and more closely separated steps as for domain II.

B. Interfaces morphology

The surfaces reported in Fig. 4(a) (corresponding to the capping layer of the TQW structures) evolve during the cooling of the sample at the end of the growth step. On the other hand, Fig. 4(b) shows the QW interfaces obtained after etching the AlAs layer in the DQW (GaAs) and NQW ($Al_{0.3}Ga_{0.7}As$) samples, as described in Sec. I, which reveal the interface morphology. As for the surfaces, we find that very different morphologies are associated with the various miscuts. Remarkably, the GaAs and $Al_xGa_{1-x}As$ interfaces are very similar. Fewer details are visible on the $Al_xGa_{1-x}As$ surface, which is probably related to a native oxide forming between the growth and the AFM measurement.

The exact sample interfaces consist of islands dispersed on the growth plane. Their diameters range between a few tens of nanometers to several hundreds of nanometers, and their geometry is roughly isotropic. Most islands are a monolayer high, but as the smaller ones are distributed on top of larger ones, the global height variation reaches several monolayers. In contrast, the 0.2°-off interfaces consist of neatly arranged parallel steps separated by about 75 nm. Although some surface effects due to the etching blur the height resolution, we can confidently state that the steps are a ML high, as this terrace width is close to the value expected for step flow on a 0.2°-off surface (80 nm). There is a vertical stripe pattern on the images of the 4°-off samples, but we cannot identify clearly the growth mode (we will call this unresolved step organization, uSO, for this reason); in this case, step flow would lead to 4-nm-wide terraces, well below our imaging resolution. Still, as attested by the cross-sectional profile, the height fluctuations of the 4°-off interfaces have amplitudes comparable to those of the exact sample. Finally, the 0.6°-off interfaces stand out from the other ones. They show the same periodic step bunching of large amplitude as that observed on the annealed surface of the TQW samples.

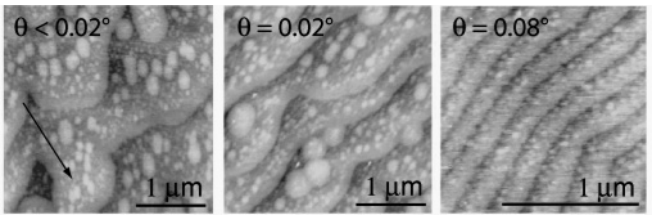

FIG. 5. Flattened AFM images showing three examples of exposed GaAs interfaces after a growth interruption of 20 s on nominally exact substrates. The local misorientations deduced from the steps separation are indicated. The arrow shows the descending direction. The full height scale is 2 nm.

C. Effect of growth interruption

We investigated the effect of a growth interruption (GI) on the morphology of the hetero-interfaces. During growth interruption, the flux of group III element precursors was stopped while the samples were still under AsH_3 flow. Several series on the same four different types of substrates were grown, with interruption either at the GaAs interface (20 s or 2 min) or at the $Al_xGa_{1-x}As$ interface (20 s). The resulting interface morphology of these vicinal samples is similar to those without GI discussed above. We observe step flow, periodic step bunching, and uSO for the 0.2°, 0.6°, and 4° samples, respectively. There is nonetheless a striking difference for nominally exact samples: while the continuously grown interface displays islands distributed over the surface, steps appear at the growth-interrupted GaAs interface. Moreover, the islands still subsist on the terraces between the steps.

Several images are presented in Fig. 5 for 20 s growth interruption at the GaAs interface of three exact samples. The respective step separation is approximately 1 μm, 700 nm, and 200 nm, corresponding to miscut angles smaller than 0.02°, 0.02°, and 0.08°. The step formation is induced by the GI. We attribute the differences to slightly different effective miscut angles. For the nearly exactly oriented surface, the steps are strongly curved and do not have a well-defined direction. Large islands appear where the terraces are broader. The largest undulations at step edge can thus be regarded as islands coalescing with, or detaching from, the upper terrace. The roughness of the step edge decreases with decreasing terrace width, and the steps become more parallel. On narrow terraces, only small islands subsist on the upper side of the terrace. Indeed, in all these images, we observe that a narrow band, about 100 nm wide, remains free from islands close to the descending step edge, indicative of the adatom surface diffusion length. Increasing the growth interruption time to 2 min does not modify these features. In particular, we see no difference concerning the island size and distribution.

In the case of 20-s GI at the $Al_xGa_{1-x}As$ interfaces, we do not observe any change as compared with continuous growth. The vicinal interfaces are similar to those reported in Fig. 4(b). As for the exact sample, in contrast to the GaAs interface, we

TABLE II. Synthesis of the correlations observed between the optical spectra and the morphology of QWs grown on substrates from different miscut angle domains. Symbols and abbreviations are defined in the text. The value quoted in the PL FWHM column is a representative value for a 15-nm QW.

Miscut domain	Morphology		Length scale	Optics	
	Surface	Interfaces		PL FWHM	μPL
I	Step flow (SF)	2D	$\xi \geqslant a_B$	1.3 meV	Sharp lines
II	Coalescent step bunching (CSB)	SF	$\xi < \xi_0$	0.6 meV	Homogeneous line
III	Periodic step bunching (PSB)	PSB	$\xi \gg a_B$	3.9 meV	Broad, distributed lines
IV	Coalescent step bunching (CSB)	uSF	$\xi < a_B$	1.2 meV	Sharp lines

do not see step formation, and the growth mode is still clearly two-dimensional.

In synthesis, we underline the three following observations: (i) the morphology of the layers strongly depends on the miscut angle of the substrate; (ii) the morphology of the GaAs and $Al_xGa_{1-x}As$ interfaces are identical, but generally differ significantly from those observed on the sample surfaces; and (iii) GI affects only the morphology of samples with a nearly exactly oriented surface.

V. CORRELATIONS BETWEEN OPTICS AND MORPHOLOGY

A. Inhomogeneous broadening, interface morphology

We identified four miscut angle domains, amongst which the QW PL linewidth varies in a significant way. To each of these domains correspond specific surface and interface morphologies. We will now discuss how the optical properties are correlated to the interface morphology. We neglect here the discussion of $Al_xGa_{1-x}As$ barrier alloy fluctuations, which will be present in all samples, but whose contribution we cannot distinguish clearly in our samples. We limit ourselves to observing that the effect of barrier alloy fluctuations will be stronger for thinner QWs (where the wave function will more strongly penetrate the barriers) than for thicker ones. Nevertheless all the observed trends in our samples are shared by all QW thicknesses (with different intensities), ruling out a major role of the barriers on the spectral evolution (while not on the absolute values involved).

In domain I, corresponding to nominally exact samples, the numerous islands at the interfaces result in a broad PL linewidth and sharp lines in μPL spectra. These sharp lines originate from the recombination of excitons localized in minima of the inhomogeneous potential. These minima are created by the width fluctuations induced by the islands, which extension ξ is larger than or of the order of the exciton Bohr radius a_B.

In domain II, the QW interfaces are characterized by narrow terraces, free of 2D islands. The corresponding PL spectra are very narrow and spatially very homogenous even at the micron level. Indeed, these terraces are larger than the exciton Bohr radius, and excitons are subject to a potential modulated mainly by the nanoroughness of the terraces. This latter modulation is much smaller than that induced by islands and occurs on a length scale inferior to a_B; it is thus averaged over the exciton spatial extension. In particular, it is not large enough to localize the excitons. One can also say with a pure topographic perspective that comparing with the case of domain I, on nominally flat samples, the system can develop island growth which effectively introduces topography changes in both directions, up and down; whereas on a vicinal surface, the set preferential slope can actually allow for flatter surfaces.

Domain III is determined by a dramatic change of the morphology of both the surface and interfaces, which all display periodic step bunching. The PL and μPL spectra are radically different than those in the other domains. The PL displays a very broad and redshifted spectrum, which corresponds to the inhomogeneous emission from several well-separated local minima, as it can be decomposed in the μPL spectra.

Domain IV is distinguished by the disappearance of periodic step bunching and the recovery of flatter interfaces, the growth mode of which cannot be resolved properly. The interfaces exhibit amplitude fluctuations comparable to those of exact samples and larger than those of 0.2°-off ones. A narrower PL linewidth is recovered in this miscut domain and does not change much up to the highest miscut investigated (8°). Its value is smaller than that of QWs grown on exact samples but slightly larger than that obtained on 0.2°-off samples. The μPL also shows features due to localized excitons but more densely distributed (spectrally) than in the case of the exact sample. For such large miscuts, the topological fluctuations are separated by distance smaller than a_B. Fluctuations are thus expected to be averaged by the exciton. The resulting effective potential is smoother and leads to a spatially more uniform emission than for exact samples. The observation of localized excitons, however, implies deep enough minima and therefore a deviation of the growth mode from pure step flow. This is consistent with the larger height fluctuations observed locally at the interfaces. These observations are summarized in Table II, where the ξ parameter is the characteristic (longitudinal) correlation length of the structure potential and ξ_0 the characteristic length giving the minimal size of an island necessary to confine an exciton, as discussed in Ref. 42.

B. Emission energy, height fluctuations

Beyond the inhomogeneous broadening and μPL peaks distribution, we now discuss the emission energy. The samples being grown together in the same growth run (thus with the same nominal QW thickness) are expected to emit at the same energy. However, this is not the case: the broader PL lines rather than the narrower lines systematically appear at a lower

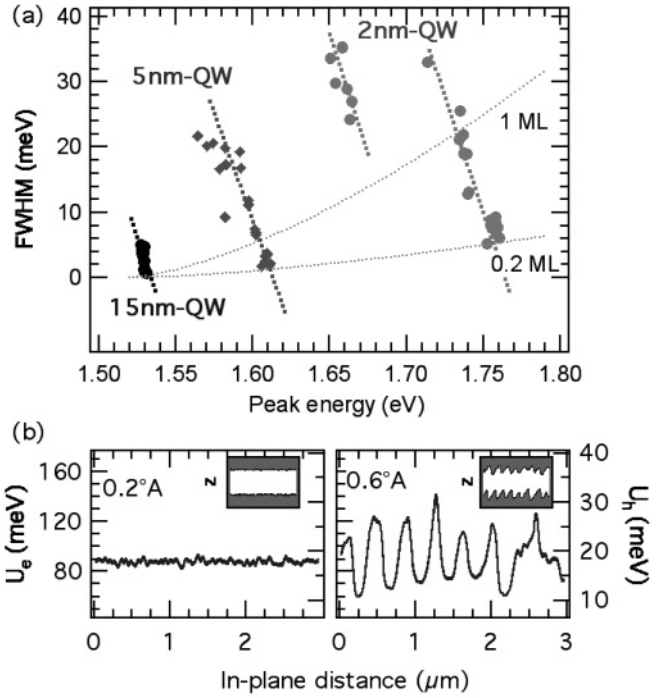

FIG. 6. (a) FWHM variations as a function of peak energy of the PL of the QWs of different thicknesses grown on substrates with various miscut. (b) Single-particle potential calculated for nominally 5-nm-thick QW, for which width is assumed to vary according to the height fluctuations measured by AFM. The extreme cases of 0.2°- and 0.6°-off samples are represented.

energy. Although there are small deviations from this behavior, the general trend is made clear in Fig. 6(a). The amplitude of the energy shift is much larger for the thinner QWs. Whereas for the 15-nm QW, the maximum redshift of 4 meV is of the order of the largest FWHM, the shift for the 5-nm QWs is as big as 47 meV and reaches 110 meV for the 2-nm QWs, which show a FWHM of 35 meV in the worst case. For these latter QWs, we observe that an ensemble of points, corresponding to the step-bunched samples, are well separated at lower energy and with larger broadening, while in the remaining cases, all points are aligned.

For the same degree of interface roughness (and barrier alloy fluctuations), the linewidth is expected to be broader for narrower QWs emitting at higher energy. Indeed, this is the tendency that we observe for the best samples, which exhibit a FWHM equivalent to fluctuations of a fraction of ML, as shown by the dotted curves in Fig. 6(a), calculated for an infinite barrier model and width fluctuations of 1 and 0.2 ML. However, within the points obtained for a given nominal thickness, the broader lines are redshifted because large fluctuations at the interfaces induce important variations of the well width; at low excitation and low temperature, only the minima of the resulting potential landscape are occupied, thus shifting the emission toward lower energies.[43] This is schematized in Fig. 6(b) for two extreme situations. The amplitude of the potentials is calculated from the height variations measured by AFM at the interfaces, reported to an average 5-nm-thick QW. The local width is converted into the single particle confinement potential, U_e (U_h) for electrons (holes), by using a simple model of a rectangular QW with finite barrier height. For the 0.2°-off sample, the minima are distributed over a few meV, homogeneously across the sample. In the case of large interface fluctuations, like those observed in 0.6°-off samples for a cross-section taken along the miscut direction, the local minima are much deeper and widely distributed, both in space and energy.

C. Lineshape, distribution of potential minima

The picture described above explains well the spectra observed in μPL: over the $\sim$1 μm large excitation spot, typically two or three local minima are visible for the 0.6°-off sample. This picture also describes the various PL lineshapes that we observe. The more deeply localized states rapidly saturate for the smoothest samples, which therefore have a smooth low-energy tail. Conversely, an extended high-energy PL tail arises from more disordered samples. The large barriers between these minima prevent thermalization of the excitons confined at different positions; thus, this tail does not correspond to a global thermal distribution; it reflects instead the distribution of local minima and their concentration at energies much lower than that corresponding to the average QW width.

The large amplitude of the height variations observed on periodic step-bunching samples is comparable to the width of the 2-nm QWs. It raises the question of the correlation of these variations between the two interfaces. The importance of interface correlation has been recently underlined in several publications[8,9,44] but was long overlooked in the discussion of the relations between interface roughness and optical properties. Ponomarev *et al*. recently demonstrated that narrow lines can be obtained, even with rough QW interfaces, if their fluctuations are correlated.[8] Indeed, in the framework of a model of local variations of the QW width, a perfect correlation would lead to a constant width. It has been shown by x-ray diffraction that step-bunched interfaces grown by MBE were correlated[45] and that growth interruption could actually be detrimental as, even though the correlation length of the disorder is increased in the QW plane, the correlation between the two interfaces in the growth direction is reduced.[46]

In our samples, the top and bottom QW interfaces have the same morphology. We can anticipate that the different growth modes observed affect differently the correlation between the two hetero-interfaces. In the case of step flow, the interfaces are obviously correlated in the sense that width fluctuations are periodic and have maximum amplitude of 1 ML (see schematic in Fig. 7). Moreover, the extension of the potential minima, related to the step advancement κ across the QW layer, is likely to be shorter than a_B. These fluctuations are thus averaged by the excitons. For 2D growth, for which islands are growing one on top of another, fluctuations may reach several monolayers. The observation of sharp lines points toward localized excitons; it implies that the interfaces are not correlated. For periodic step bunching as well, the observation of deep potential minima indicates an absence of correlation between the two interfaces. Whether it implies a quenching of the nominally 2-nm-thick QW layer or not is nevertheless an open question.

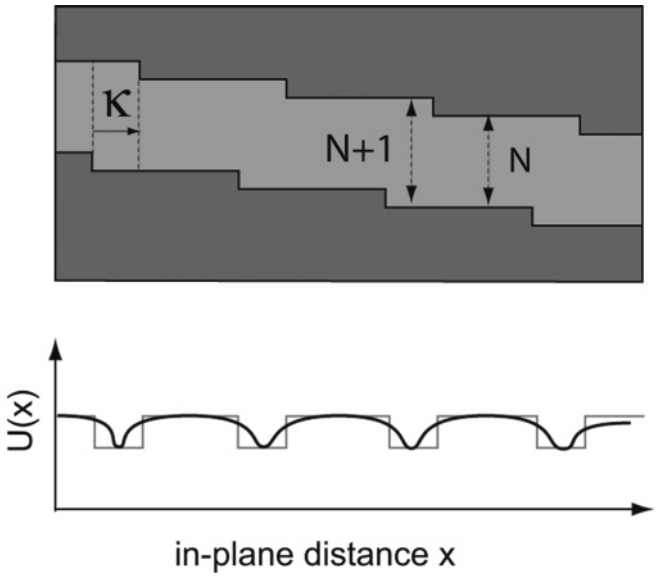

FIG. 7. Schematic representation of the effect of the correlation between the interfaces in the case of step flow. Variations in the QW width correspond to the variation of the effective potential sketched below.

VI. GROWTH MODES AND GROWTH KINETICS

The observation of several growth modes within a short range of substrate miscut angle is remarkable. In particular, we underline that, in the same system, islanding and pure step flow coexist at close to zero miscut (i.e. sample characterized by large terraces), while evolving to step-bunched instability at larger misorientation. Also noticeable is the fact that both the GaAs and the $Al_xGa_{1-x}As$ layers have similar morphologies, at least on a few nanometers scale. The observation that the GaAs interface morphology does not significantly depend on the QW thickness is a natural consequence of this similarity between GaAs and $Al_xGa_{1-x}As$. Indeed, theoretical studies show that often several hundreds of ML have to be grown before reaching a steady state of the growth front.[47] This condition is always satisfied in our samples as we grew a thick buffer prior to depositing the structures.

Let us now discuss the formation mechanisms of the different morphologies that we observed. For almost flat substrates (domain I), the evolution of the interface with growth interruption (Fig. 5) shows that the morphology is determined by the finite migration velocities: steps form only during GI. A similar evolution of macrosteps with GI time was already reported for MOVPE.[30] In that study, growth was performed at a lower temperature (625 °C) and with a different As source (TBA), which may explain differences in growth kinetics. Nevertheless, Bernatz *et al.*[30] observed a continuous evolution of the steps up to 2 min of GI and remaining islands on the annealed surface. We surprisingly did not observe any evolution between 20 s and 2 min growth interruption; we still observed islands in between the steps. In contrast to the apparently steady-state islands between steps obtained during growth, the flat terraces that were obtained on annealed surface raise the question of the possible significant role of atom detachment from steps at our rather high growth temperature.

Similar considerations can be made for the morphology of the domain II sample, which shows step flow during growth, but coalescent step bunching at the relaxed surface. In general, the pure step flow that we observed at the interface is obtained when the migration length of ad species is larger than the step separation. The migration length is roughly given by the island-free (denuded) zone at the step edge (∼100 nm).

The evolution to a coalescent step-bunching morphology on the surface is less intuitive, and a number of proposals have been put forward to explain this phenomenology. Shinohara *et al.* studied experimentally the occurrence of step bunching at the surface of GaAs layers grown by MOVPE on slightly misoriented substrates.[27,29] They observed step flow for small miscuts and coalescent step bunching above a critical transition angle. At a lower growth temperature and using B-misoriented substrates, they obtained step flow on 0.5°-off surfaces.[48] They found that the critical angle decreases with increasing temperature and proposed a model based on the saturation of the Ga atoms at steps by the adatoms and on the desorption of atoms from the surface. According to this model and to their experiments, step bunching occurs at a smaller angle during annealing than during growth. The exact formation mechanism of coalescent step bunching is still unclear in their modeling, although a proposal, which relies on desorption and exchange of adatoms between steps, has been put forward to describe the formation of step branching during annealing (and not during growth)[49] of a deoxidized GaAs surface.

The denuded zone observed at the lower terrace edge of growth-interrupted samples can be interpreted as indicative of a negative Erlich–Schwoebel (ES) barrier. This is, however, inconsistent with the step flow observed for small terrace width. Instead, it can be evidence of the preferential precursor decomposition at the steps from where the released adatoms diffuse. Indeed, the inclusion of precursors allows us to mimic the effect of a negative ES barrier. A similar morphology of periodic step bunching that we observed has been modeled first by Pimpinelli *et al.*, albeit without focusing particularly on the MOVPE system, who considered both precursors and adatoms kinetics.[47,50,51] In their assumptions, they calculated that a thick layer (of the order of 100 ML) has to be grown before the instability sets in. They also predict that once the growing surface has evolved to the bunched state, no coarsening of the bunches happens, and the morphology remains stable. Indeed, the morphology that we observed on the TQW surface, thus several hundreds of ML above the QW, is still identical.

Noticeable in Ref. 50, one can find a hint for the reason as to why step bunching sets in when increasing the miscut angle (decreasing the terrace length). The step-bunching instability is described as a function of the product ζl, where ζ is an increasing function of the dissociation rate of the precursors υ_p and decreases with the precursors diffusivity D_p. Here, l is the average terrace width. The instability shows up for large enough ζl. Although it is not accounted for by the model, the cracking υ_p of the precursors should increase with increasing miscut, as the steps play a catalytic role. Since, at the same time, l decreases, the product behavior might be therefore nonmonotonous with the miscut.

Along similar lines, Chua *et al.* have recently addressed this issue specifically for the case of MOVPE of GaAs layers, in particular concentrating on the cap morphology.[52]

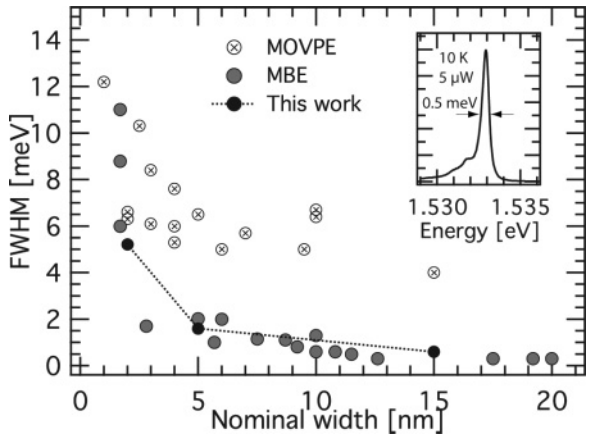

FIG. 8. Overview of the best PL linewidth of GaAs/$Al_xGa_{1-x}As$ QWs of different widths (and various x) reported in the literature.[2,20–23,29,41,46,53–61] Crossed (gray) points are for MOVPE (MBE)-grown samples. The points corresponding to the values discussed in this paper are reported in black. The inset shows 15-nm QW spectra with record narrow linewidth.

The model explicitly takes into account both the precursors and adatoms kinetics via the use of Burton–Cabrera–Frank (BCF)-type equations. The main result of that analysis is that the mechanism responsible for the transition to step bunching is the difference in the molecular decomposition rates at steps, which produces a net downhill current, as would an inverse ES barrier, combined with the decomposition of the precursors on the terraces. Without terrace decomposition (and in the absence of desorption), the model predicts that step flow is always unstable against step bunching.[52]

VII. CONCLUSION

In this paper, we presented and discussed the dramatic effects of the miscut angle of vicinal substrates on the properties of GaAs/$Al_xGa_{1-x}As$ QWs grown by MOVPE. With regard to the optical properties, large fluctuations of the PL and PLE spectra linewidth are observed over small miscut angle ranges. They can be unambiguously attributed to the modification of the growth mode of the epitaxial layers. Several different types of hetero-interfaces disorder can thus be created, making this kind of sample a model system for studies using more advanced characterization methods.[9] In particular, we demonstrated that very homogeneous interfaces can be obtained when growing on substrates with a small miscut angle. The optical quality of these samples is such that excitonic complexes can be resolved.

As shown in Fig. 8, such QW quality was previously reserved for samples grown by MBE. In contrast to the objective usually pursued with this later technique, we highlighted the fact that micron-large smooth areas are not necessary to reach high optical quality. Oppositely, it appears that an excellent configuration occurs when the natural length scale imposed by the miscut angle is smaller than the diffusion length of the adatoms but longer than the excitonic Bohr radius. A necessary condition is nevertheless that the growth takes place in the step-flow mode, which results in interfaces free of atomic islands and with steps whose correlation ensures a smooth excitonic potential.

However, we observed that step-flow mode is maintained only in a narrow angle range. The transition from one growth mode to another was discussed in view of the existing models and of our AFM images. The additional observation that GI has an effect on the interface morphology only on nearly exactly (001)-oriented substrates and not on vicinal surfaces should help to refine models and to quantify the kinetic variables of the growth mechanisms.

In summary, we presented a complete study of the optics, morphology, and growth kinetics of GaAs/$Al_xGa_{1-x}As$ QWs grown by MOVPE. We described the modification of the properties when using vicinal substrates and how an appropriate choice of substrate and growth conditions allows reaching very high-quality QWs. The fine understanding of the relation between optics and morphology and of the sensitivity of morphology on growth parameters sets important guidelines for further progress in MOVPE growth.

*Present address: Tyndall National Institute, University College Cork, Cork, Ireland; Corresponding author: emanuele.pelucchi@tyndall.ie
†Present address: CNRS, LPN, Laboratoire de Photonique et de Nanostructures, F-91460 Marcoussis, France.

[1] C. Weisbuch, R. Dingle, A. C. Gossard, and W. Wiegmann, Solid State Commun. **38**, 709 (1981).
[2] D. C. Reynolds, K. K. Bajaj, C. W. Litton, P. W. Yu, W. T. Masselink, R. Fisher, and H. Morkoá, Appl. Phys. Lett. **46**, 51 (1985).
[3] C. A. Warwick, W. Y. Jan, A. Ourmazd, and T. D. Harris, Appl. Phys. Lett. **56**, 2666 (1990).
[4] A. Ourmazd, D. W. Taylor, J. Cunningham, and C. W. Tu, Phys. Rev. Lett. **62**, 933 (1989).
[5] D. Gammon, B. V. Shanabrook, and D. S. Katzer, Phys. Rev. Lett. **67**, 1547 (1991).
[6] M. A. Herman, D. Bimberg, and J. Christen, J. Appl. Phys. **70**, R2 (1991).
[7] R. Zimmermann, F. Grosse, and E. Runge, Pure Appl. Chem. **69**, 1179 (1997).
[8] I. V. Ponomarev, L. I. Deych, and A. A. Lisyansky, Phys. Rev. B **71**, 155303 (2005).
[9] V. Savona and W. Langbein, Phys. Rev. B **74**, 075311 (2006).
[10] J. Singh and K. K. Bajaj, J. Appl. Phys. **57**, 5433 (1985).
[11] R. L. Schwoebel, J. Appl. Phys. **37**, 3682 (1966).
[12] R. L. Schwoebel, J. Appl. Phys. **40**, 614 (1968).
[13] H. Metiu, Y. T. Ylu, and Z. Zhang, Science **255**, 1088 (1992).
[14] N. Néel, T. Maroutian, L. Douillard, and H. J. Ernst, Phys. Rev. Lett. **91**, 226103 (2003).
[15] G. Danker, O. Pierre-Louis, K. Kassner, and C. Misbah, Phys. Rev. Lett. **93**, 185504 (2004).
[16] H. Omi and Y. Homma, Phys. Rev. B **72**, 195322 (2005).
[17] A. Ballestad and T. Tiedje, Phys. Rev. B **74**, 153405 (2006).

[18]M. Yoon, H. N. Lee, W. Hong, H. M. Christen, Z. Zhang, and Z. Suo, Phys. Rev. Lett. **99**, 055503 (2007).
[19]H. Castella and J. W. Wilkins, Phys. Rev. B **58**, 16186 (1998).
[20]M. Yoshita, H. Akiyama, L. N. Pfeiffer, and K. W. West, Appl. Phys. Lett. **81**, 49 (2002).
[21]C. W. Tu, R. C. Miller, B. A. Wilson, P. M. Petroff, T. D. Harris, R. F. Kopf, S. K. Sputz, and M. G. Lamont, J. Cryst. Growth **81**, 159 (1987).
[22]K. T. Shiralagi, R. A. Puechner, K. Y. Choi, R. Droopad, and G. N. Maracas, J. Cryst. Growth **114**, 337 (1991).
[23]K. Leosson, J. R. Jensen, W. Langbein, and J. M. Hvam, Phys. Rev. B **61**, 10322 (2000).
[24]M. Tanaka and H. Sakaki, J. Appl. Phys. **64**, 4503 (1988).
[25]T. Shitara, D. D. Vvendesky, M. R. Wilby, J. Zhang, J. H. Neave, and B. A. Joyce, Phys. Rev. B **46**, 6825 (1992).
[26]M. Shinohara, M. Tanimoto, H. Yokoyama, and N. Inoue, J. Cryst. Growth **145**, 113 (1994).
[27]M. Shinohara and N. Inoue, Appl. Phys. Lett. **66**, 1936 (1995).
[28]A. Rudra, E. Pelucchi, D. Oberli, N. Moret, B. Dwir, and E. Kapon, J. Cryst. Growth **272**, 615 (2004); E. Pelucchi, N. Moret, B. Dwir, D. Y. Oberli, A. Rudra, N. Gogneau, A. Kumar, E. Kapon, E. Levy, and A. Palevski, J. Appl. Phys. **99**, 093515 (2006); V. Dimastrodonato, L. O. Mereni, R. J. Young, and E. Pelucchi, J. Cryst. Growth **312**, 3057 (2010).
[29]M. Shinohara, H. Yokoyama, and N. Inoue, J. Vac. Sci. Technol. B **13**, 1773 (1995).
[30]G. Bernatz, S. Nau, R. Rettig, and W. Stolz, J. Electron. Mater. **29**, 129 (2000).
[31]N. Moret, D. Y. Oberli, E. Pelucchi, N. Gogneau, A. Rudra, and E. Kapon, Appl. Phys. Lett. **88**, 141917 (2006).
[32]G. Bernatz, S. Nau, R. Rettig, H. Jänsch, and W. Stolz, J. Appl. Phys. **86**, 6752 (1999).
[33]P. Borri, M. Gurioli, M. Colocci, F. Martelli, M. Capizzi, A. Patané, and A. Polimeni, J. Appl. Phys. **80**, 3011 (1996).
[34]F. Martelli, A. Polimeni, A. Patanè, M. Capizzi, P. Borri, M. Gurioli, M. Colocci, A. Bosacchi, and S. Franchi, Phys. Rev. B **53**, 7421 (1996).
[35]J. B. B. De Oliveira, E. A. Meneses, and E. C. F. da Silva, Phys. Rev. B **60**, 1519 (1999).
[36]V. Srinivas, Y. J. Chen, and E. C. Wood, Solid State Commun. **89**, 611 (1994).
[37]N. N. Sibeldin, M. L. Shorikov, and V. A. Tsvetkov, Nanotechnology **12**, 591 (2001).
[38]F. J. Teran, L. Eaves, L. Mansouri, H. Buhmann, D. K. Maude, M. Potemski, M. Henini, and G. Hill, Phys. Rev. B **71**, 161309(R) (2005).
[39]A. S. Bracker, E. A. Stinaff, D. Gammon, M. E. Ware, J. G. Tischler, D. Park, D. Gershoni, A. V. Filinov, M. Bonitz, F. M. Peeters, and C. Riva, Phys. Rev. B **72**, 035332 (2005).
[40]A. V. Filinov, C. Riva, F. M. Peeters, Y. E. Lozovik, and M. Bonitz, Phys. Rev. B **70**, 035323 (2004).
[41]S. Glasberg, G. Finkelstein, H. Shtrikman, and I. Bar-Joseph, Phys. Rev. B **59**, R10425 (1999).
[42]N. Moret, EPFL Thesis No 4070 (2008) and references therein.
[43]R. Zimmermann and E. Runge, J. Lumin. **60-61**, 320 (1994).
[44]G. Kocherscheidt, W. Langbein, and V. Savona, Phys. Status Solidi B **238**, 486 (2003).
[45]E. A. Kondrashkina, S. A. Stepanov, R. Opitz, M. Schmidbauer, R. Köhler, R. Hey, M. Wassermeier, and D. V. Novikov, Phys. Rev. B **56**, 10469 (1997).
[46]L. Gottwaldt, K. Pierz, F. J. Ahlers, E. O. Göbel, S. Nau, T. Torunski, and W. Stolz, J. Appl. Phys. **94**, 2464 (2003).
[47]A. Videcoq, A. Pimpinelli, and M. Vladimirova, Appl. Surf. Sci. **177**, 213 (2001).
[48]K. Ikuta, M. Shinohara, and N. Inoue, Jpn. J. Appl. Phys. **34**, L220 (1995).
[49]K. Hata, H. Shigekawa, T. Okano, T. Ueda, and M. Akiyama, Phys. Rev. B **55**, 7039 (1997).
[50]K. Hata, H. Shigekawa, T. Okano, T. Ueda, and M. Akiyama, Phys. Rev. B **55**, 7039 (1997).
[51]A. Pimpinelli, R. Cadoret, E. Gil-Lafon, J. Napierala, and A. Trassoudaine, J. Cryst. Growth **258**, 1 (2003).
[52]A. L. S. Chua, E. Pelucchi, A. Rudra, B. Dwir, E. Kapon, A. Zangwill, and D. D. Vvedensky, Appl. Phys. Lett. **92**, 013117 (2008).
[53]R. F. Kopf, E. F. Schubert, T. D. Harris, and R. S. Becker, Appl. Phys. Lett. **58**, 631 (1991).
[54]R. D. Dupuis, J. G. Neff, and C. J. Pinzone, J. Cryst. Growth **124**, 558 (1992).
[55]D. Schmitz, G. Strauch, J. Knauf, H. Jürgensen, M. Heyen, and K. Wolter, J. Cryst. Growth **93**, 312 (1988).
[56]Y. Horikoshi, Semicond. Sci. Technol. **8**, 1032 (1993).
[57]H. Kawai, K. Kaneko, and N. Watanabe, J. Appl. Phys. **56**, 463 (1984).
[58]N. Kobayashi, T. Makimoto, Y. Yamauchi, and Y. Horikoshi, J. Appl. Phys. **66**, 640 (1989).
[59]N. Watanabe and Y. Mori, Surf. Sci. **174**, 10 (1986).
[60]N. Inoue, K. Ikuta, M. Shinohara, and J. Osaka, J. Cryst. Growth **146**, 379 (1995).
[61]F.-Y. Juang, Y. Nashimoto, and P. K. Bhattacharya, J. Appl. Phys. **58**, 1986 (1985).